International Journal of Impact Engineering 59 (2013) 29–37

Contents lists available at SciVerse ScienceDirect

International Journal of Impact Engineering

journal homepage: www.elsevier.com/locate/ijimpeng

A statistical description of explosion produced debris dispersion

M.M. van der Voort [a,*], J. Weerheijm [a,b]

[a] TNO, Dep. Explosions, Ballistics and Protection, P.O. Box 45, 2280 AA Rijswijk, The Netherlands
[b] Faculty of Civil Engineering and Geosciences, Delft University of Technology, The Netherlands

ARTICLE INFO

Article history:
Received 17 December 2012
Received in revised form
20 January 2013
Accepted 4 March 2013
Available online 26 March 2013

Keywords:
Explosion
Detonation
Risk
Debris
Dispersion
Throw

ABSTRACT

The handling of explosives and ammunition introduces a safety risk for personnel and third parties. Accidents related to storage, transport and transshipment may result in severe injury and material damage. Dispersion of structural debris is one of the main hazards resulting from detonations inside structures. Reliable prediction models for debris dispersion are essential for risk assessment methods.

In this article we give a statistical description of the dispersion of explosion produced debris. The basis is a general expression for the projectile areal number density in the horizontal and vertical plane. Combined with engineering models for the launch conditions, predictions can be made. An analytical solution to the equations of motion may be used to allow for fast calculations. A parameter study shows consistent results. The model has been validated with internal detonation tests of bare charges in reinforced concrete structures. The validation clearly shows the prediction capabilities of the model for three loading regimes described in the literature.

We give a thorough description of the validity and limitations of the model, and an outlook of current and future research. Examples are the failing debris mass distribution prediction for reinforced concrete in the shock overloading regime, and ricochet and roll and break-up at impact phenomena.

1. Introduction

The handling of explosives and ammunition introduces a safety risk for personnel and third parties. Accidents related to storage, transport and transhipment may result in severe injury and material damage. A detailed account of such an event is described by Kummer [1] for a Swiss ammunition storage accident. In a risk assessment both the causes and consequences of accidents are analysed. This enables the comparison of risk reduction measures related to prevention and mitigation.

The prediction of the consequences of explosions starts with a prediction of the physical effects, such as blast and debris throw from the storage structure or container. While blast wave propagation is a relatively well understood phenomenon, less information is available on the break-up process and dispersion of debris. A direct consequence is that current safety distances (AASTP-1 [2]) are mainly empirically based. Physical models that capture the main phenomena are required to make extrapolations possible, for example towards structure dimensions and stored quantities different from those tested.

An impression of an explosive event creating a debris hazard is given in Fig. 1 (Grønsten [3]). This illustrates an internal detonation test in a reinforced concrete structure. During the last decades many such tests have been carried out with various building materials and dimensions. The amount of data collected with debris pick-up and high speed camera has largely increased over the years, providing a valuable database for model validation. Experimental and theoretical research in this area has been coordinated and conducted within the Klotz Group, an international group of explosives safety experts.

Prediction models for debris dispersion that are both reliable and fast running are essential for risk assessment methods. Models with a varying level of detail and application can be found in the literature. For the debris hazard of stored explosives and ammunition, models are described in AASTP-4 [4]. An example is the Klotz Group Engineering Tool (van der Voort et al. [5]). Other existing approaches are based on Monte Carlo simulations (Häring [6]) or numerical dynamic response and break-up calculations by Wang [7], and Weerheijm et al. [8]. In the field of range safety, Gan et al. [9] has developed a detailed trajectory model. For debris created during industrial accidents like vessel ruptures, models from Mebarki et al. [10,11], Pula et al. [12], and the Yellow Book [13] have been described.

In this article we present a model for the dispersion of explosion produced debris, with a focus on above ground reinforced concrete

* Corresponding author. Tel.: +31 0888661288.
E-mail address: martijn.vandervoort@tno.nl (M.M. van der Voort).

0734-743X/$ – see front matter © 2013 Elsevier Ltd. All rights reserved.
http://dx.doi.org/10.1016/j.ijimpeng.2013.03.002

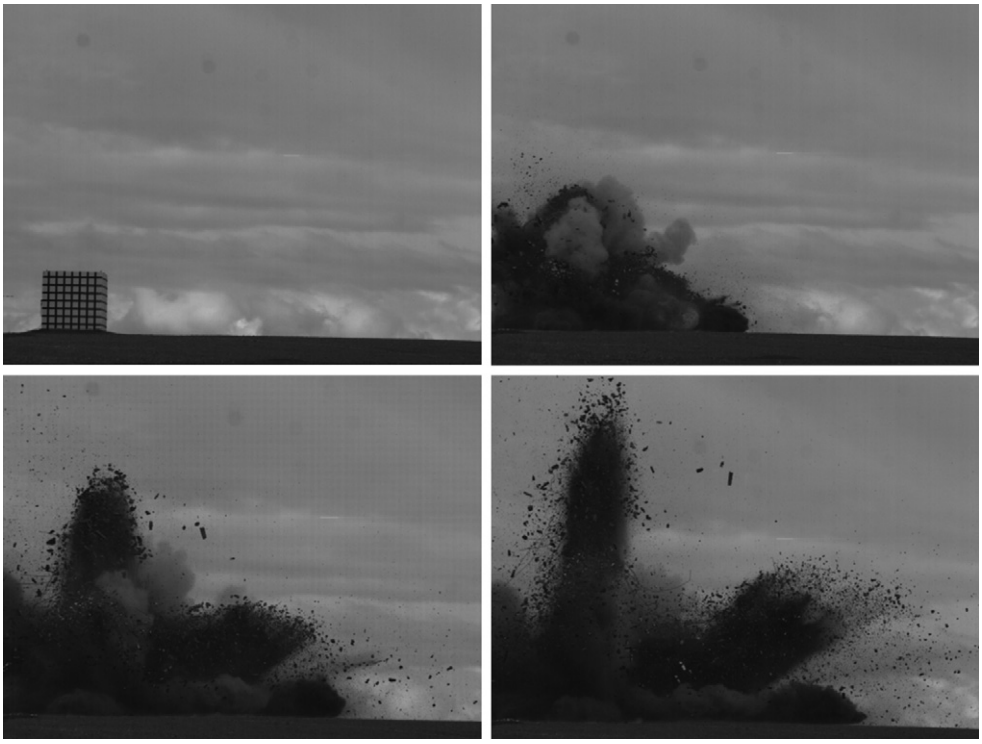

Fig. 1. Debris hazard created during the detonation of 6.9 kg TNT equivalent in an 8 m^3 Kasun structure (Grønsten [3]). Four frames from high speed camera are shown from left to right, top to bottom.

structures. In Section 2 the source function theorem is presented which is an extension of theory described by van der Voort et al. [14]. The result is a general expression for the projectile areal number density in the horizontal and vertical plane. Engineering models for the launch conditions and trajectories are discussed in Section 3. In Section 4 we validate the model by comparing it to experimental data. The limitations of the model, and an outlook of current and future research are described in Section 5. In Section 6 conclusions are drawn.

2. Theory

2.1. The source function

We consider a structural element (e.g. a wall) which breaks up during an internal explosion. This structural element can be considered as a source of projectiles (Fig. 2). The element has a height H, a width W, thickness t, and mass M.

Among the projectiles, variations in launch velocity (U), launch direction (azimuthal angle β, vertical launch angle α), and initial location in the wall (x, y, z) are present. Furthermore the ballistic properties of the projectiles are variable, such as their shape and mass (m). For projectiles with a compact shape an appropriate variable to represent the ballistic behaviour is the typical size or length (L) of the projectiles:

$$L = \left(\frac{m}{\rho}\right)^{1/3} \tag{1}$$

In this equation ρ is the projectile density. Examples of compact projectiles are debris from concrete and masonry walls. A more detailed description of the debris shape is given in Section 3.

Because the amount of projectiles is typically very large it makes sense to define a probability density function for all variables that describe the initial launch conditions; the source function $n(x,y,z,L,U,\alpha,\beta)$. The amount of projectiles dN that is launched from an infinitesimal part of a wall (dx, dy, dz) with velocities between U and $U + \mathrm{d}U$, launch angles between α and $\alpha + \mathrm{d}\alpha$, azimuthal angles between β and $\beta + \mathrm{d}\beta$, and typical projectile lengths between L and $L + \mathrm{d}L$, can be formulated as:

$$\mathrm{d}N = n(x,y,z,L,U,\alpha,\beta)\cdot\cos(\alpha)\cdot\mathrm{d}x\cdot\mathrm{d}y\cdot\mathrm{d}z\cdot\mathrm{d}L\cdot\mathrm{d}U\cdot\mathrm{d}\alpha\cdot\mathrm{d}\beta \tag{2}$$

The cosine term is related to the spherical coordinate system defined by α and β. The source function has to fulfil a normalization requirement. This means that when it is integrated over all relevant ranges of the variables we should obtain the total number of launched projectiles from the source (N).

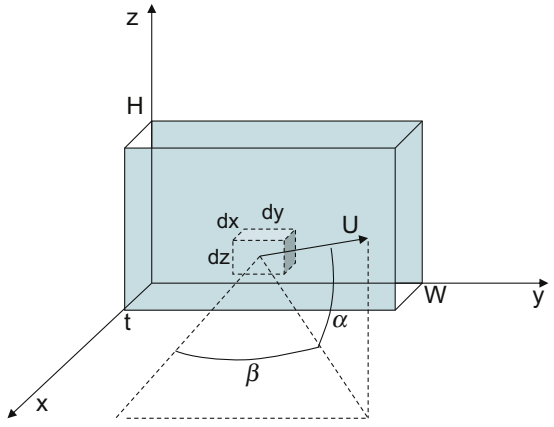

Fig. 2. Illustration of the variables used to describe a wall, including an infinitesimal part.

$$\int_{-\pi}^{\pi}\int_{-\pi/2}^{\pi/2}\int_{0}^{\infty}\int_{0}^{\infty}\int_{0}^{H}\int_{0}^{W}\int_{0}^{t} n(x,y,z,L,U,\alpha,\beta)\cdot\cos(\alpha)\cdot dx\cdot dy\cdot dz\cdot dL\cdot dU\cdot d\alpha\cdot d\beta = N \quad (3)$$

The total number of projectiles is directly related to the mass distribution and mass of the structural element. This will be further addressed in Section 3.

For the current application not all of these variables are relevant:

- We are interested in the dispersion of projectiles over a large distance. For this situation the wall can be modelled as a point source at location (x_0, y_0, z_0). This can be for example a location in the centre of the wall, or at ground level.
- Internal detonation tests show that concrete slabs are typically accelerated as a whole before disintegrating into separate debris pieces (Lim et al. [24]). For this situation we can assume that all projectiles have an equal launch velocity U_0, which does not vary with mass nor launch angle.
- Experimental evidence shows that the correlation between launch direction and debris mass is not significant (Kummer [20]). We may therefore assume that the mass distribution is independent of launch angle.

With these simplifications the source function can be written as:

$$n(x,y,z,L,U,\alpha,\beta) = n_1(L)\cdot n_2(\alpha,\beta)\cdot\delta(x-x_0)\cdot\delta(y-y_0)\cdot\delta(z-z_0)\cdot\delta(U-U_0) \quad (4)$$

In this equation δ is the Kronecker delta function, with the following property:

$$\int_{x_1}^{x_2}\delta(x-x_0)\cdot dx = 1 \text{ for } x_1 < x-x_0 < x_2 \quad (5)$$

This means that requirement Eq. (3) reduces to:

$$\left(\int_{0}^{\infty} n_1(L)\cdot dL\right)\cdot\left(\int_{-\pi}^{\pi}\int_{-\pi/2}^{\pi/2} n_2(\alpha,\beta)\cdot\cos(\alpha)\cdot d\alpha\cdot d\beta\right) = N \quad (6)$$

By convention it is required that the projectile length integral should equal N. As a result:

$$\int_{0}^{\infty} n_1(L)\cdot dL = N \quad (7)$$

And for the angular integral we require that it equals 1.

$$\int_{-\pi}^{\pi}\int_{-\pi/2}^{\pi/2} n_2(\alpha,\beta)\cdot\cos(\alpha)\cdot d\alpha\cdot d\beta = 1 \quad (8)$$

2.2. The source function theorem

The source function theorem gives an expression for the projectile areal number density in both the horizontal and vertical plane (number of impacting projectiles per unit of area). Ignoring the Kronecker delta functions in Eq. (4), Eq. (2) can be rewritten as:

$$dN = n_1(L)\cdot n_2(\alpha,\beta)\cdot\cos(\alpha)\cdot dL\cdot d\alpha\cdot d\beta \quad (9)$$

This is the number of projectiles launched through an angular window determined by $d\alpha$ and $d\beta$ in an interval of projectile length dL. We consider the impact of projectiles in an infinitesimal element of area in the horizontal plane ($dA = r\cdot dr\cdot d\beta$) and vertical plane ($dS = r\cdot dz\cdot d\beta$) at a distance r. This is illustrated in Fig. 3.

The projectile areal number density can be formulated by dividing dN by the relevant element of area. It should be noted that by doing this the factor $d\beta$ cancels out, and a derivative with respect to r is introduced. Furthermore we have to integrate over the range of projectile lengths of interest ($L_1 \le L \le L_2$). If we consider all projectiles, $L_1 = 0$ and $L_2 \to \infty$.

For the projectile areal number density in the horizontal plane we can write:

$$\Phi_h(r,\beta) = \frac{dN}{dA} = \int_{L_1}^{L_2}\frac{n_1(L)\cdot n_2(\alpha(r,L),\beta)\cdot\cos(\alpha(r,L))}{r}\cdot\frac{d\alpha(r,L)}{dr}\cdot dL \quad (10)$$

In this equation $\alpha(r,L)$ gives a relation between the launch angle and the projectile impact distance and length. This function follows from the properties of projectile trajectories, and therefore also depends on other factors like the projectile launch velocity and the drag coefficient which have not been indicated explicitly as functional dependencies here.

In Eq. (10) the function inside the integral:

$$\Phi_h(r,\beta) = \frac{N\cdot n_2(\alpha(r,L),\beta)\cdot\cos(\alpha(r,L))}{r}\cdot\frac{d\alpha(r,L)}{dr} \quad (11)$$

can be recognized as a 'Green function'; an expression for the projectile areal number density for a source of N projectiles with equal projectile length.

For the projectile areal number density in the vertical plane we can derive an equation similar to Eq. (10):

$$\Phi_v(r,z,\beta) = \frac{dN}{dS} = \int_{L_1}^{L_2}\frac{n_1(L)\cdot n_2(\alpha((r,z,L),\beta)\cdot\cos(\alpha(r,z,L))}{r}\cdot\frac{d\alpha(r,z,L)}{dz}\cdot dL \quad (12)$$

Note that here the dependency on the height in the vertical plane has been added, and the derivative has to be taken with respect to z.

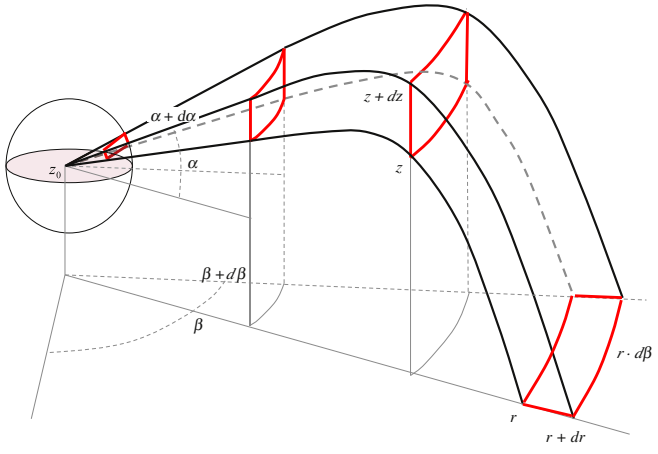

Fig. 3. Illustration of the source function theorem.

In this section we derived a general expression for the projectile areal number density in the horizontal and vertical plane. These quantities are directly related to the hazard for an exposed person. In order to make predictions possible, more information is needed about the launch conditions. These are the projectile mass or length distribution, the velocity and the angular distribution. Furthermore trajectory calculations are required. Recently developed engineering models are able to provide this information, and are described in Section 3.

3. Engineering models

In this section we present a number of engineering models for the projectile launch conditions and trajectories. These will make it possible to make predictions with the theory presented in Section 2.

3.1. Length distribution

In the literature many types of distributions for the size and mass of debris and fragments are reported. A recent overview is given by Elek and Jaramaz [15]. One class of distributions takes the form:

$$n(>m) \sim e^{-(m/\mu)^{\lambda}} \tag{13}$$

This is the generalized Mott distribution. The original Mott distribution (Mott [16], Ballistics and Gunnery [17]) follows from two-dimensional geometric statistics, and is valid for thin walled ductile structures like ammunition shells. For this case $\lambda = 1/2$. Break-up of brittle materials like concrete and masonry is typically a three dimensional process for which $\lambda = 1/3$ is an appropriate value.

From these considerations an exponential distribution of debris length can be expected. In Section 2.1 the typical projectile length L was already introduced. For the probability density function we can write:

$$n_1(L) = \frac{N}{L_{av}} \cdot e^{-L/L_{av}} \tag{14}$$

This equation satisfies Eq. (7).

The average debris mass can be related to the average debris length as follows:

$$m_{av} = \frac{1}{N} \int_0^{\infty} \rho \cdot L^3 \cdot n_1(L) \cdot dL = 6 \cdot \rho \cdot {L_{av}}^3 \tag{15}$$

From the conservation of mass follows that the total number of debris should equal:

$$N = \frac{M}{m_{av}} \tag{16}$$

As an example Fig. 4 shows two experimentally determined cumulative length distributions from the US Eskimore test program; the Sci Pan 4 and 5 test (Conway et al. [18,19]). A cumulative length distribution shows the number of debris with a length larger than a certain value. During these tests respectively 1000 and 3000 kg of TNT were detonated in a structure with various types of concrete walls. The length, width and height were about 9 by 9 by 3 m. In the order of 10^4 concrete debris pieces per wall were picked-up, individually weighted and GPS located. The measured debris masses were divided in mass bins, translated to length bins, and a data fit with a reasonable quality could be determined. Fig. 4 clearly shows that for the same wall type, a larger Net Explosive Quantity (NEQ) leads to a steeper slope and hence a smaller average length.

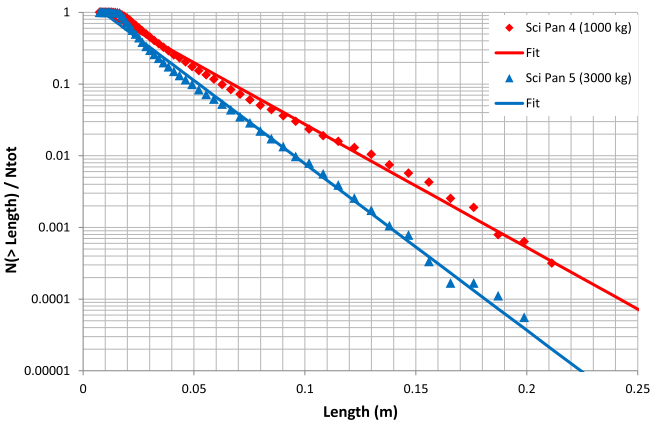

Fig. 4. Experimentally determined cumulative debris length distribution for the Sci Pan 4 and 5 test (Conway et al. [18,19]). Results for a CMU (Concrete Masonry Unit) wall. Data and exponential fit have been normalized by the total number of picked up debris.

The determination of the average length L_{av} has been carried out for numerous large and small scale internal detonation experiments. Among these experiments variations in NEQ, internal volume (V) and wall thickness (t) were present. Currently, only empirical relations are available to relate the average length to these variables. An example is shown in Fig. 5. The parameter combination plotted on the horizontal axis is classified, and has therefore not been included in this paper.

3.2. Angular distribution

Also the angular distribution of wall debris can be obtained from debris pick-up. The test data shows a strong directionality which can be represented by a bivariate normal distribution (Kummer [20]). For the azimuthal angle β the distribution is centred around the wall normal direction, while for the launch angle α the distribution has a slight upward tilt.

$$n_2(\alpha,\beta) = \frac{1}{2\pi \cdot \sigma_\alpha \cdot \sigma_\beta} \cdot e^{-(\alpha-\alpha_{av})^2/2\cdot{\sigma_\alpha}^2} \cdot e^{-(\beta-\beta_{av})^2/2\cdot{\sigma_\beta}^2} \tag{17}$$

For relevant launch angles the cosine term in Eq. (8) is to a good approximation equal to 1. In this case the above equation satisfies this requirement. As an example Fig. 6 shows an experimentally determined azimuthal debris distribution, together with a reasonable data fit to a normal distribution.

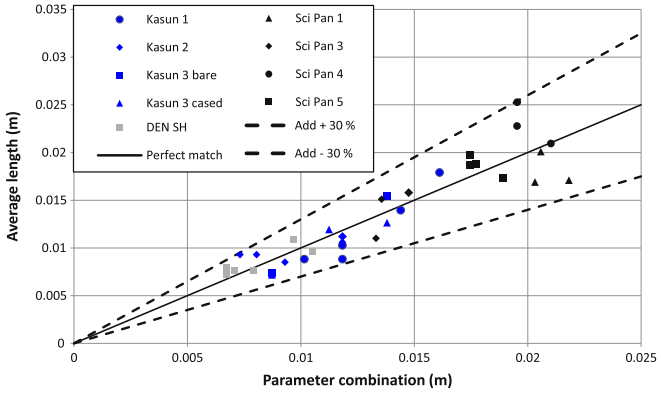

Fig. 5. Average length as a function of a parameter combination, consisting of NEQ, internal volume and wall thickness.

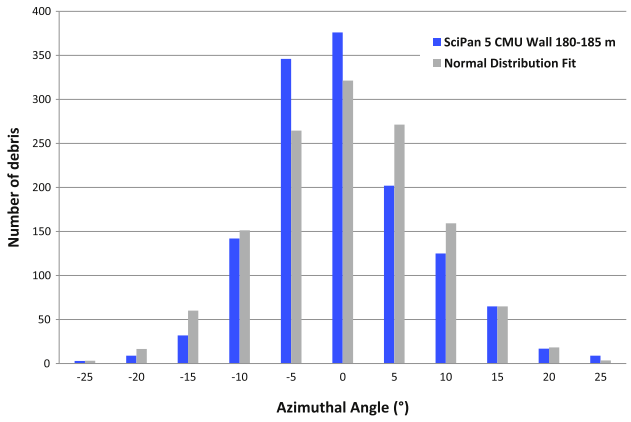

Fig. 6. Azimuthal debris distribution observed in the Sci Pan 5 test in a range interval between 180 and 185 m from a CMU wall (Conway et al. [19]). The wall normal direction is located at 0°. A normal distribution data fit is included.

3.3. Launch velocity

In Section 2.1 it has been assumed that the launch velocity U_0 is a constant for all projectiles. The launch velocity has been investigated in a large amount of slab launch tests by Dörr et al. [21]. During these tests slabs with variable mass were launched from a 1 m^3 box, after internal detonations with variable NEQ. This resulted in the so called Debris Launch Velocity (DLV) formula (Van Doormaal et al. [22]).

$$\mathrm{DLV} = C \cdot \sqrt{\frac{\mathrm{NEQ}}{V^{2/3} \cdot \rho \cdot t}} \tag{18}$$

In this equation V is the internal volume, ρ the wall density, t is the wall thickness, and $C = 525$ m/s. Velocities measured in full scale tests (Berglund et al. [23], Lim et al. [24], and Grønsten et al. [3]), and dynamic response calculations (Lu et al. [25]) yield a reasonable comparison.

3.4. Trajectory calculations

The trajectories of projectiles are governed by air drag and gravity. In general the lift force can be neglected for all practical situations. At this stage it is assumed that the trajectories of the numerous projectiles are mutually independent; they do not influence one another. This gives the following equation of motion:

$$\frac{\mathrm{d}\vec{U}}{\mathrm{d}t} = \frac{1}{m} \cdot \left(\vec{F}_{\mathrm{drag}} + \vec{F}_{g} \right) \tag{19}$$

The forces and their components are illustrated in Fig. 7.

This equation can be written as a series of two coupled differential equations:

$$\begin{aligned} \frac{\mathrm{d}u}{\mathrm{d}t} &= -\kappa \cdot \sqrt{u^2 + v^2} \cdot u \\ \frac{\mathrm{d}v}{\mathrm{d}t} &= -\kappa \cdot \sqrt{u^2 + v^2} \cdot v - g \end{aligned} \tag{20}$$

In these equations u and v are the horizontal and vertical velocity component respectively. The ballistic coefficient κ can be formulated as follows:

$$\kappa = \frac{A_{\perp} \cdot \rho_a \cdot C_D}{2 \cdot m} = \frac{S_N \cdot \rho_a \cdot C_D}{2 \cdot \rho^{2/3} \cdot m^{1/3}} = \frac{S_N \cdot \rho_a \cdot C_D}{2 \cdot \rho \cdot L} = \kappa(L) \tag{21}$$

g: gravitational acceleration
ρ_a: density of air
$A_{\perp}$: average presented projectile area
C_D: drag coefficient (in general a function of Mach number)
S_N: shape number

Eq. (21) shows that the ballistic coefficient is inversely proportional to the typical projectile length (Eq. (1)). This means that a larger projectile causes a smaller deceleration. As a result a larger projectile will reach a further distance compared to a smaller projectile, when launched with equal velocity.

The equations of motion have to be integrated numerically in general. The first reason is the fact that the equations are coupled. Furthermore, the drag coefficient is in general a function of the Mach number, and can not be treated as a constant.

However, for relatively small velocities and flat trajectories (closely around the wall normal direction) an analytical solution exists; the horizontal drag approximation, Eq. (22) (Van der Voort et al. [26]). This solution has the same basis as other solutions found in literature (Carlucci and Sidney [27] & Ballistics and Gunnery [17]).

$$R = \frac{1}{\kappa} \cdot \ln\left(1 + \frac{2 \cdot \kappa \cdot {U_0}^2 \cdot \alpha}{g} \right) \tag{22}$$

This equation gives the impact distance R as a function of launch velocity and launch angle for a launch from ground level ($z_0 = 0$ m). The limitation to relatively flat trajectories (small launch angles) is the same under which Eq. (17) is valid. For compact projectiles the shape number may vary between 1 for a face-on cube, 1.2 for a sphere, and around 2 for natural fragments from warheads. For concrete debris an appropriate shape number is 1.5 (Van der Voort et al. [5]). At subsonic velocities the drag coefficient for debris can be approximated with a constant value of about 0.8. Ricochet and roll phenomena are not considered at this stage, i.e. the impact location is assumed to be the final resting place.

A comparison between Eq. (22) and the full numerical solution of Eq. (20) is given in Fig. 8 for three debris lengths. The graph shows that the curves all tend to the no drag solution (parabola) for small launch velocities. The horizontal drag approximation results in an overestimation of the impact distances for larger velocities. Dependent on the application a certain deviation might be acceptable.

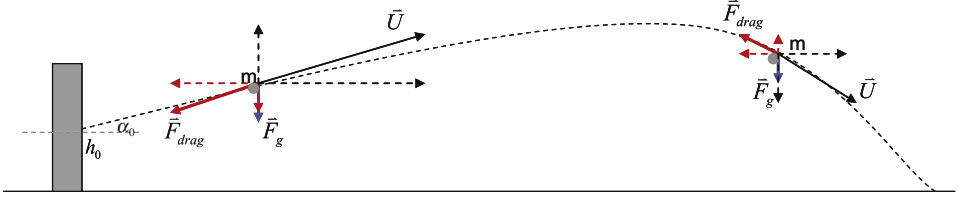

Fig. 7. Illustration of forces acting on projectiles during their trajectory.

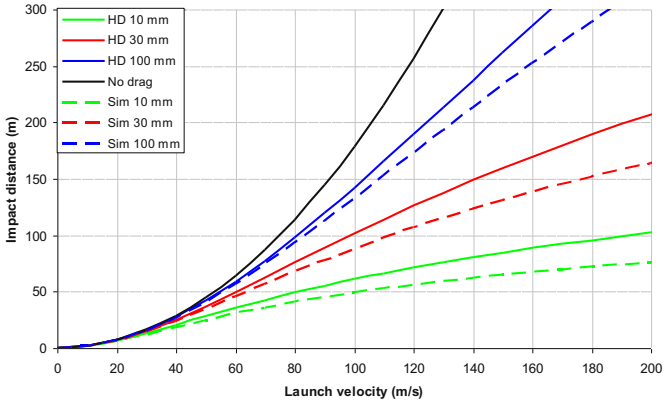

Fig. 8. Impact distance as a function of initial velocity for three debris lengths. Comparison between horizontal drag approximation (HD) and numerical solution ($z_0 = 0$ m, $\alpha_0 = 5\,^\circ$, $C_D = 0.8$, $S_N = 1.5$). The parabola represents the solution without drag.

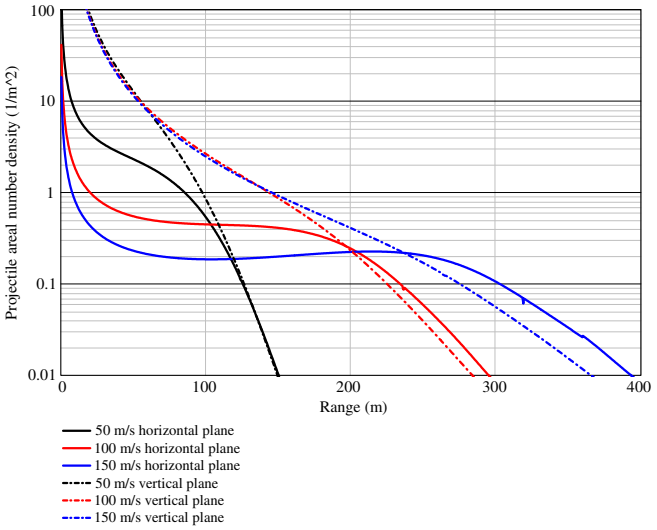

Fig. 9. Debris areal number density in the horizontal and vertical plane versus range for three launch velocities. Results are shown in the wall normal direction.

In order to calculate the projectile areal number density, Eq. (22) has to be inverted to give $\alpha(r,L)$:

$$\alpha(r,L) = \frac{g\cdot\left(e^{\kappa(L)\cdot r}-1\right)}{2\cdot\kappa(L)\cdot {U_0}^2} \tag{23}$$

and

$$\frac{\mathrm{d}\alpha(r,L)}{\mathrm{d}r} = \frac{g\cdot e^{\kappa(L)\cdot r}}{2\cdot {U_0}^2} \tag{24}$$

In a similar way we have:

$$\frac{\mathrm{d}\alpha(r,L)}{\mathrm{d}z} = \frac{\kappa(L)}{e^{\kappa(L)\cdot r}-1} \tag{25}$$

3.5. Illustration of model predictions

The source function theorem can be combined with the engineering models presented above to obtain closed-form expressions for the projectile areal number density in the horizontal and vertical plane. For this purpose Eqs. (10) and (12) have been combined with information about the length distribution (Eqs. (14)–(16)), the angular distribution (Eq. (17)), and trajectories (Eqs. (23)–(25)). This enables us to perform parameter studies and to make model predictions.

This is illustrated with the break-up of a 2 by 2 m reinforced concrete wall with a thickness of 15 cm. We assume a typical average debris length of 10 mm, and consider only debris larger than 30 mm. This means that the integration in Eqs. (10) and (12) runs from 30 mm up to infinity. The integration has been carried out with MathCad software. Fig. 9 shows the debris areal number density in the horizontal and vertical plane versus range for launch velocities of 50, 100, and 150 m/s.

The figure shows that the debris areal number density extends further outwards for larger launch velocities. The curves for the horizontal plane drop down for larger launch velocities, because the same amount of debris is dispersed over a larger area. For 50 m/s the debris areal number density shows a monotonic decrease with distance, while for 150 m/s a maximum occurs. This accumulation is caused by air drag.

The curves for the vertical plane coincide at short distances. In this regime the trajectories are well approximated by a straight line, and are hence independent of launch velocity. At short distances the curves for the vertical plane are one to two orders of magnitude larger than for the horizontal plane. In this regime the hazard from low angle high velocity debris is much larger for a standing person than for a laying person.

In the far field the curves for the horizontal and vertical plane approach one another. In this regime the impact angle is relatively steep, and the hazard for a standing person is comparable to that for a laying person.

This illustration shows that the model yields consistent results for variations in launch velocity. Other parameter studies can be conducted for the average length, the minimum pick-up length, the angular distribution parameters, the drag coefficient and the shape number.

4. Validation

In this section we validate the model (i.e. the combination of the source function theorem and engineering models) by comparing it to test data.

4.1. Loading regimes

A large variety of building dimensions and stored NEQ are found in practice. Up to a loading density in the order of 0.1 kg/m^3 most structures are able to contain the explosion. The extent of this regime is very much dependent on reinforcement properties and the presence of vent openings. The described model is not suitable for this regime. Beyond this point, Weerheijm et al. [28] has identified three loading regimes:

- The gas pressure overloading regime reaches up to a loading density of about 1 kg/m^3. In this regime the structural response is important. The debris velocity is typically below 100 m/s.
- The blast impulsive overloading regime reaches up to 16 kg/m^3, where launch velocities up to 300 m/s may occur.
- In the shock overloading regime, beyond 16 kg/m^3, the break-up is determined by local effects. Launch velocities may reach well into the supersonic regime. A significant part of the structure breaks up in aggregate size debris or dust.

In order to have a representative validation, we have compared model predictions for tests in all three loading regimes.

4.2. Test description

For the validation, the model has been applied to a number of internal detonation tests with bare charges in Kasun ammunition storage structures. These are 8 m^3 cubical reinforced concrete structures with a 15 cm wall thickness. The tests were performed by Berglund et al. [23] and Grønsten et al. [3]. After the tests debris larger than about 30 mm was picked up in collection zones centred around the wall normal directions. From this data the average length has been determined with a fit procedure. The debris areal number density versus range was determined as well. The standard deviation in the azimuthal angle was determined for some of the tests where debris was also picked up for off normal directions. The results are shown in Table 1.

4.3. Calculation settings

Table 2 gives the values for the model parameters that have been used in the calculations. For the average length, values have been calculated with the empirical relation described in Section 3.1. These values do not deviate more than about 10% from the measured average lengths in Table 1. For the launch velocity (U_0) the DLV equation (Eq. (18)) has been applied, except for the 6.9 kg test which required a relatively large velocity to match the test data. The mean launch angle was assumed to be 5°, which is an average value of a large amount of tests (Kummer [20]). For the standard deviation in the azimuthal angle an average value from the Kasun tests has been used. It was further assumed that this value is also applicable to the (vertical) launch angle.

4.4. Comparison

In Fig. 10 the experimentally determined debris areal number density in the horizontal plane is plotted together with model predictions for the various tests. Model predictions are determined by numerical integration of Eq. (10) from a minimum pick-up length of respectively 10, 20, 30, 40, and 50 mm up to infinity. The test data has to be compared to the model predictions for debris larger than 30 mm (black curve). In each figure the five model predictions coincide in the far field which shows that only the largest debris pieces reach these distances.

The relatively high velocity required to match the 6.9 kg test is a common feature for the gas pressure overloading regime. Due to the structural response, the break-up of the structure and venting starts a late stage, causing a relatively high kinetic energy transfer (Lim et al. [24]).

The 20 and 80 kg test are situated in the blast impulsive overloading regime. The model predictions and test data show comparable behaviour. Local deviations may be caused by ricochet and roll phenomena which are not included in the model.

Table 2
Model parameters used for the calculations.

NEQ (kg)	L_{av} (mm)	DLV (m/s)	U_0 (m/s)	Mean launch angle (°)	Standard deviation in azimuthal angle and launch angle (°)
6.9	14.0	36	52	5	9
20	12.0	62	62	5	9
20	12.0	62	62	5	9
80	9.96	124	124	5	8
110	9.55	145	145	5	8
160	9.08	175	175	5	8

For the 110 kg, and especially the 160 kg test, the model overestimates the debris areal number density at most distances. This is a common feature for the shock overloading regime, where a significant part of the wall breaks up into aggregate size debris or dust. The exponential length distribution (Eq. (14)) is only valid for a fraction of the wall mass.

5. Discussion

In this section a number of model limitations are discussed in more detail, and an outlook of current and future research is given.

At the higher end of the blast impulsive overloading regime the horizontal drag approximation will loose its validity. A numerical solution to the equations of motion and a Mach dependent model for the drag coefficient are required here. The Klotz Group has developed an engineering tool which takes this into account (van der Voort et al. [5]). The equations of motion have to be integrated for various launch angles and mass or length bins (i). A common mass bin system is the Sci Pan system (Tatom et al. [29]), which has also been used for the pick-up in many experiments. In this case the function $\alpha(r,L_i)$ has to be obtained through interpolation. The debris areal number density in the horizontal plane for mass bin '*i*' can be formulated as an adaptation of Eq. (11).

$$\Phi_{hi}(r,\beta) = \frac{N_i \cdot n_2(\alpha(r,L_i),\beta)\cdot\cos(\alpha(r,L_i))}{r}\cdot\frac{\mathrm{d}\alpha(r,L_i)}{\mathrm{d}r} \tag{26}$$

In this equation L_i is the representative length for bin '*i*', while N_i is the total number of debris in bin *i*. The aggregation of debris densities from the various mass bins can be performed by summing over '*i*', instead of integrating over debris length (Eq. (10)).

In the shock overloading regime a significant part of the wall breaks up into aggregate size debris or dust. The exponential length distribution (Eq. (14)) is only valid for a fraction of the wall mass. Current research in the Klotz Group is aimed at developing models for the deviation of the length distribution at high loading densities.

In the presented model it is assumed that the mutual influence of debris can be neglected. In the initial stages of the launch, the debris is part of a dense debris cloud which moves more easily

Table 1
Specification and results of Kasun tests. Berglund et al. [23] and Grønsten et al. [3].

NEQ (kg)	Loading density (kg/m^3)	Charge location	Minimum pick-up distance (m)	Measured L_{av} (mm)	Measured standard deviation in azimuthal angle (°)
6.9	0.86	Floor centre	25	15.4	Rear: 7.8 Side: 9.4
20	2.5	Floor centre	70	10.6	–
20	2.5	Centre, mid height	70	11.2	–
80	10	Floor centre	70	8.5	–
110	13.8	Floor centre	25	7.35	Rear: 7.5 Side: 8.7
160	20	Floor centre	70	9.3	–

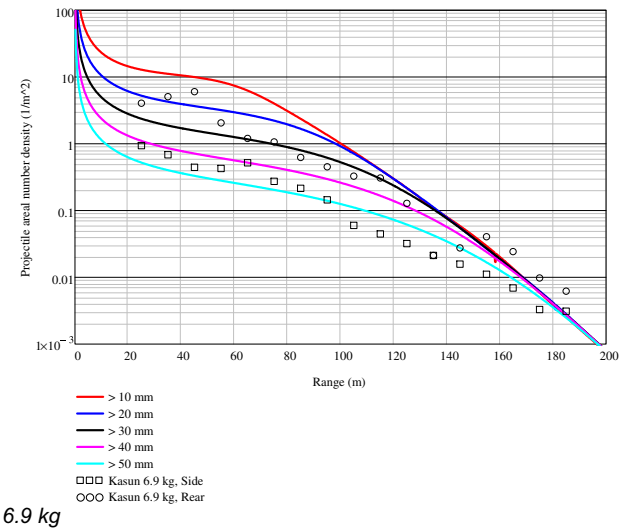

6.9 kg

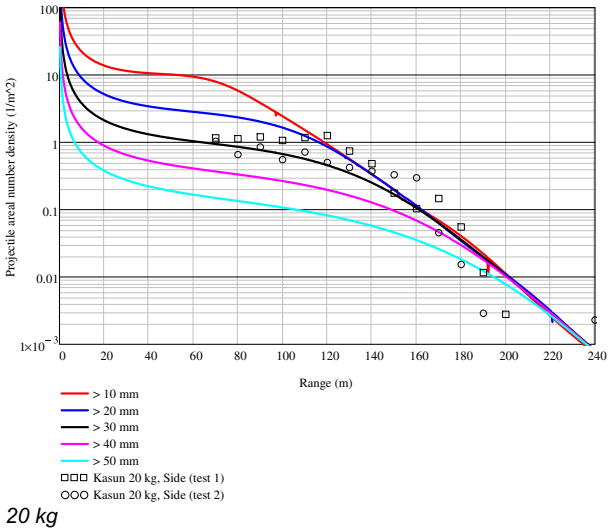

20 kg

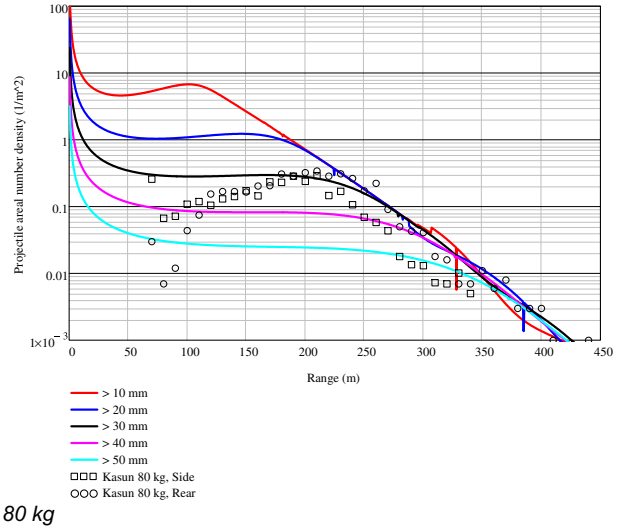

80 kg

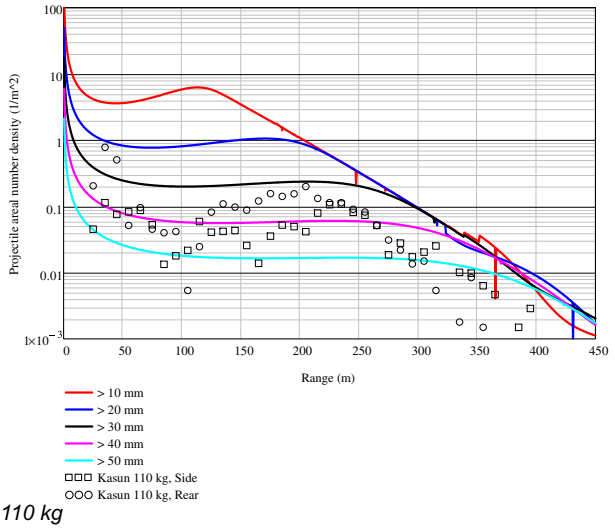

110 kg

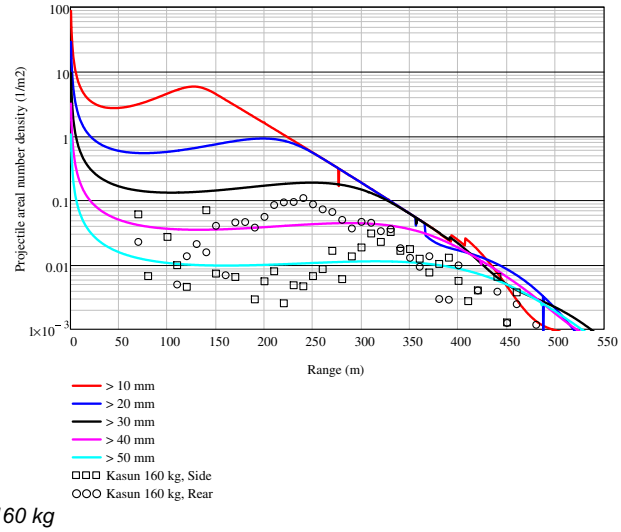

160 kg

Fig. 10. Debris areal number density versus range for a Kasun test with respectively 6.9, 20, 80, 110 and 160 kg explosives. Model predictions for various minimum pick-up sizes. Experimental data in two wall normal directions, both with a minimum pick-up size of 30 mm.

through air than individual pieces of debris. As the debris cloud expands the debris exits the cloud and moves independently. For this mechanism the ballistic filtering model was developed. This model has also been implemented in the KG Engineering Tool (but was not included in the validation in Section 4).

From high speed video we have evidence that ricochet and roll and break-up at impact play an important role. To assess the hazard posed by debris it may be important to take these effects into account. Bounce and roll is neglected in the current approach where all impact distances are based on first impact. This may result in unrealistic launch conditions when performing backward calculations. Experimental studies on bounce and roll were executed by Knock et al. [30]. Break-up at impact is a phenomenon which poses problems to the usability of experimentally determined mass distributions. The mass distribution obtained from pick-up data is not equal to the distribution during flight. Fundamental studies in break-up at impact are currently being carried out by the Klotz Group.

For compact debris such as concrete and masonry the debris length is an appropriate variable to represent the ballistic behaviour. This is not the case for debris generated by steel ISO containers. In this case most of the debris is plate-like and has a fixed thickness. As a result its ballistic coefficient is more or less mass (and length) independent. On the other hand the ballistic behaviour is strongly dependent on the type of motion (tumbling, face-on, or edge-on). For plate-like debris the theory presented in this article would need to be reformulated.

6. Conclusions

A statistical description of the dispersion of explosion produced debris has been presented. The basis is a general expression for the projectile areal number density in the horizontal and vertical plane. Combined with engineering models for the launch conditions, predictions can be made. An analytical solution to the equations of motion may be used to allow for fast calculations. A parameter study shows consistent results.

The model has been validated with internal detonation tests of bare charges in reinforced concrete structures. The validation clearly shows the prediction capabilities of the model for three loading regimes described in literature. In the shock overloading regime the model overestimates the debris areal number density. In this regime a significant part of a reinforced concrete wall breaks up into aggregate size debris or dust. Current research in the Klotz Group is aimed at developing models for the deviation of the length distribution at high loading densities. Other improvements are being made by taking into account the mutual influence of debris during their trajectories, and break-up at impact phenomena and ricochet and roll.

Acknowledgements

We would like to acknowledge the Klotz Group for which part of this work was conducted. Our special thanks for FOI (Sweden), NDEA (Norway), and DDESB (USA) for the availability of experimental data.

References

[1] Kummer PO. Evaluation of the debris throw from the 1992 explosion in the Steingletscher installation in Switzerland. Journal of Hazardous Materials 1997;56:149–67.
[2] AASTP-1. Manual of NATO safety principles for the storage of military ammunition and explosives, change 2. Brussel: Allied Ammunition Storage and Transport Publication; May 2006.
[3] Grønsten GA, Berglund R, Carlberg A, Forsén R. Break up tests with small “ammunition houses” using cased charges – Kasun III. FOI-R– 2479 –SE. Forsvarsbygg Report 68/2009. FOI and Forsvarsbygg. ISSN 1650–1942. Technical report April 2009.
[4] AASTP-4. Manual on explosives safety risk analysis. Part I and II, Change 2. 1st ed. Allied Ammunition Storage and Transport Publication; October 2011.
[5] Van der Voort MM, Radtke FKF, van Amelsfort RJM, Khoe YS, Stacke I, Voss M, et al. Recent developments of the KG software. In: 34th DoD explosives safety seminar. Portland, Oregon: DDESB; 2010.
[6] Häring I. Quantitative hazard and risk analysis for fragments of, high explosive events. Risk, Reliability and Societal Safety 2007.
[7] Wang Ming, Hao Hong, Ding Yang, Li Zhong-Xian. Prediction of fragment size and ejection distance of masonry wall under blast load using homogenized masonry material properties. International Journal of Impact Engineering 2009;36:808–20.
[8] Weerheijm J, Stolz A, Riedel W, Mediavilla J. Modelling loading and break-up of RC structure due to internal explosion of fragmenting shells. MABS 2012.
[9] Gan W, Chrostowski JD. 3D fragment throw simulation to determine fragment density and impact on buildings. In: 34th DoD explosives safety seminar. Portland, Oregon: DDESB; 2010.
[10] Mebarki A, Nguyen QB, Mercier F, Ami Saada R. Structural fragments and explosions in industrial facilities. Part I: probabilistic description of the source terms. Journal of Loss Prevention in the Process Industries 2009;22:408–16.
[11] Mebarki A, Nguyen QB, Mercier F, Ami Saada R. Structural fragments and explosions in industrial facilities. Part II: projectile trajectory and probability of impact. Journal of Loss Prevention in the Process Industries 2009;22:417–25.
[12] Pula R, Khan FI, Veitch B, Amyotte PR. A model for estimating the probability of missile impact: missiles originating from bursting horizontal cylindrical vessels. Process Safety Progress June 2007;26(2). http://dx.doi.org/10.1002/prs.10178.
[13] Methods for the calculations of physical effectsPublicatiereeks Gevaarlijke Stoffen 2 (PGS 02). The Hague: Ministerie van VROM; November 2005.
[14] Van der Voort MM, Van Doormaal JCAM, Verolme EK, Weerheijm J. A universal throw model and its applications. International Journal of Impact Engineering 2008;35:109–18. http://dx.doi.org/10.1016/j.ijimpeng.2007.01.004.
[15] Elek P, Jaramaz S. Fragment mass distribution of naturally fragmenting warheads. FME Transactions 2009;37(3):135.
[16] Mott NF, Linfoot EH. A theory of fragmentation. British Ministry of Supply Report, AC 3348 1943.
[17] Textbook of ballistics and gunnery Part I, basic theory, application and design, vol. 1. London: Her Majesty's Stationery Office; 1987.
[18] Conway RT, Tatom JW, Swisdak MM. Sci Pan 4: program description and test results. In: 34th DoD explosives safety seminar. Portland, Oregon: DDESB; 2010.
[19] Conway RT, Tatom JW. Sci Pan 5 quick-look briefing, presented to the Klotz group. Fall 2011 Meeting 18–20 October 2011. NAVFAC.
[20] Kummer P. Debris throw from magazine walls due to explosions, debris, launch angle. NATO AC/326(SG6)(SWI)IWP 059-06, TM 204-11 7 February 2006. BK&P.
[21] Dörr A, Michael K, Gürke G. Experimental investigations of the debris launch velocity from internally overloaded concrete structures. Final Report DLV 4-2002. Institut Kurzzeitdynamik Ernst-Mach-Institut; 2002.
[22] van Doormaal JCAM, Dörr A, Forsen R. Debris launch velocity program DLV. In: 11th international symposium on the interaction of the effects of munitions with structures May 2003. ISIEMS.
[23] Berglund R, Carlberg A, Forsén R, Grønsten GA, Langberg H. Break up tests with small “ammunition houses” – Kaun II. FOI-R– 2202 –SE. Forsvarsbygg Report 51/06. FOI and Forsvarsbygg. ISSN 1650–1942. Technical report December 2006.
[24] Lim HS, Koh YH, Grønsten GA. Analysis of the Kasun II – break up tests with small “ammunition houses”. In: 33rd DoD explosives safety seminar. Palm Springs, California: DDESB; 2008.
[25] Lu Yong, Xu Kai. Prediction of debris launch velocity of vented concrete structures, under internal blast. International Journal of Impact Engineering 2007;34:1753–67. http://dx.doi.org/10.1016/j.ijimpeng.2006.09.096.
[26] Van der Voort MM, Verolme EK, Weerheijm J. The application of debris and fragment throw models in risk assessment methodologies. In: 33rd DoD explosives safety seminar. Palm Springs, California: DDESB; 2008.
[27] Carlucci DE, Sidney SJ. Ballistics, theory and design of guns and ammunition. CRC Press; 2008.
[28] Weerheijm J, van Doormaal JCAM, Guerke G, Lim HS. The break-up of ammunition magazines, failure mechanisms and debris distribution. In: 33rd DoD explosives safety seminar 2002. DDESB.
[29] Tatom JW, Davis JS, Conway RT. Continued study of the SAFER/SciPan mass bin concept. In: 34th DoD explosives safety seminar. Portland, Oregon: DDESB; 2010.
[30] Knock C, Horsfall I, Champion SM, Harrod IC. The bounce and roll of masonry debris. International Journal of Impact Engineering 2004;30:1–16.